PCCP

PAPER

View Article Online
View Journal | View Issue

Cite this: *Phys. Chem. Chem. Phys.*, 2019, **21**, 22022

The tetracapped truncated tetrahedron in 16-vertex tetrametallaborane structures: spherical aromaticity with an *isocloso* rather than a *closo* skeletal electron count†

Amr A. A. Attia,[a] Alexandru Lupan,*[a] R. Bruce King*[b] and Sundargopal Ghosh*[c]

Density functional theory studies on the experimentally known $Cp^*_3Rh_3B_{12}H_{12}Rh(B_4H_9RhCp^*)$ as well as the model compounds $Cp_4Rh_4B_{12}H_{12}$ and $Cp_3Rh_3B_{12}H_{12}Rh(\eta^3\text{-}C_3H_5)$ indicate low energy structures with central Rh_4B_{12} tetracapped tetratruncated tetrahedra (TTT) for these 32 Wadean skeletal electron systems. This skeletal electron count corresponds to $2k^2$ (k = 4) skeletal electrons suggesting a spherical aromatic system with filled 1s + 1p + 1d + 1f molecular orbitals as well as an *isocloso* $2n$ (= 32 for n = 16) skeletal electron count. Similar TTT structures are found for the valence isoelectronic 32 skeletal electron systems $[Cp_4M''_4B_{12}H_{12}]^{4+}$ (M″ = Ni, Pd, Pt) and $[Cp_4M'_4B_{12}H_{12}]^{4-}$ (M′ = Fe, Ru, Os). The preferred structures of the 34 skeletal electron systems $[Cp_4M_4B_{12}H_{12}]^{2-}$ (M = Co, Rh, Ir), $[Cp_4M''_4B_{12}H_{12}]^{2+}$ (M″ = Ni, Pd, Pt) are not the most spherical TTT despite their $2n$ + 2 skeletal electron count (= 34 for n = 16) for a *closo* structure by the Wade–Mingos rules. Instead they are prolate (elongated) polyhedra with two degree 6 and two degree 5 metal vertices with a central M_4 macrobutterfly having one long M···M distance of ~5.0 Å between the wingtips. The preferred structures for the still electron richer 36 skeletal electron systems $Cp_4M''_4B_{12}H_{12}$ (M″ = Pd, Pt) are derived from triple square antiprisms with two open M''_2B_2 square faces. A distorted version of this polyhedron is the deltahedral structure with four degree 5 metal vertices and four degree 6 boron vertices found in the valence isoelectronic 36 skeletal electron first row transition metal derivatives $Cp_4Ni_4B_{12}H_{12}$ and $[Cp_4Co_4B_{12}H_{12}]^{4-}$. However, this polyhedron is not found in the 36 skeletal electron $[Cp_4M_4B_{12}H_{12}]^{4-}$ (M = Rh, Ir), that instead have symmetrical central M_4B_{12} TTTs. For some 16-vertex $[Cp_4M_4B_{12}H_{12}]^z$ systems deviating from the favored 32 skeletal electron count, low-energy structures are found in which hydrogen atoms migrate to bridge B–B edges or bend over to bridge M–B edges. In addition, the hypoelectronic hexacations $[Cp_4M_4B_{12}H_{12}]^{6+}$ (M = Co, Rh, Ir; Ni, Pd, Pt) are found to have low-energy structures in which three of the four Cp rings are hydrogenated to give tetrahapto cyclopentadiene $\eta^4\text{-}C_5H_6$ rings.

Received 31st July 2019,
Accepted 20th September 2019

DOI: 10.1039/c9cp04263f

rsc.li/pccp

1. Introduction

The formation of stable borane[1] and carborane[2] cages based on the most spherical *closo* deltahedra was first realized experimentally in the 1960s. However, the 12-vertex icosahedron was the largest such borane or carborane cage to be synthesized until the 2003 report by Welch and coworkers[3] of the 13-vertex dicarbaborane 1,2-μ-$(CH_2)_3$-3-Ph-1,2-$C_2B_{11}H_{10}$ in which the carbon atoms were fixed in adjacent positions by a $-CH_2CH_2CH_2-$ bridge. Shortly thereafter a similar principle was used to synthesize the 14-vertex deltahedral dicarbaborane $(\mu\text{-}CH_2)_3C_2B_{12}H_{12}$.[4] Larger borane structures such as $B_{18}H_{22}$ do not have structures based on a single polyhedron but on a fusion of two or more polyhedra.

The most spherical *closo* deltahedra in borane structures having 6 to 12 vertices with the exception of the 11-vertex deltahedron have exclusively degree 4 and 5 vertices, where the number of edges meeting at a given vertex is its degree (Fig. 1). The 11-vertex *closo* deltahedron is an exception since it is topologically required to have a single degree 6 vertex in addition to its eight degree 5 vertices and two degree 4 vertices.[5] Degree 6 vertices also are necessarily required in the most spherical deltahedra with more than 12 vertices.

[a] *Faculty of Chemistry and Chemical Engineering, Babeş-Bolyai University, Cluj-Napoca, Romania. E-mail: alupan@chem.ubbcluj.ro*
[b] *Department of Chemistry, University of Georgia, Athens, Georgia, 30602, USA. E-mail: rbking@chem.uga.edu*
[c] *Department of Chemistry, Indian Institute of Technology Madras, Chennai, India. E-mail: sghosh@iitm.ac.in*

† Electronic supplementary information (ESI) available. See DOI: 10.1039/c9cp04263f

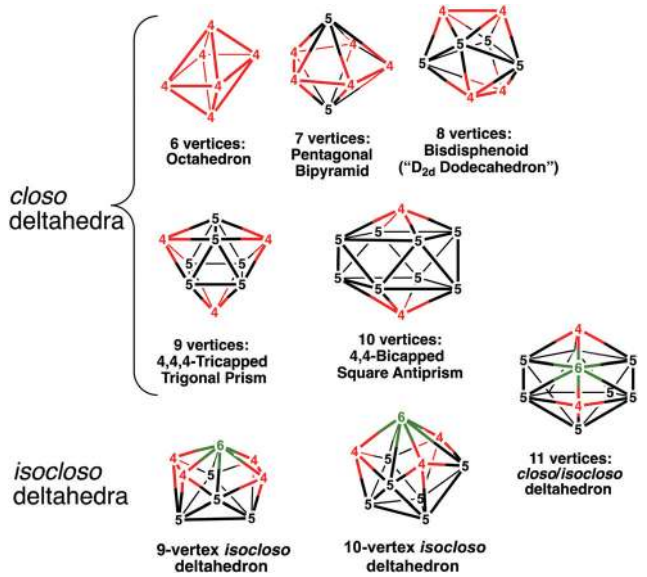

Fig. 1 A comparison of *closo* and *isocloso* deltahedra having from 6 to 11 vertices.

The Frank–Kasper 14-, 15- and 16-vertex deltahedra (Fig. 2), other than the regular icosahedron as a trivial example, have exclusively degree 5 and 6 vertices with no pair of adjacent degree 6 vertices.[6] The most spherical 13-vertex deltahedron is an exception since it necessarily has one degree 4 vertex in addition to ten degree 5 vertices and two degree 6 vertices. In a sense it is the inverse of the most spherical 11-vertex deltahedron relative to the regular icosahedron. The 16-vertex Frank–Kasper deltahedron, namely the tetracapped truncated tetrahedron, is a natural upper limit since larger most spherical deltahedra necessarily have adjacent degree 6 vertices or vertices of degree 7 or higher.

The Wade–Mingos rules[7–9] suggest favored structures based on *n*-vertex *closo* deltahedra to have $2n + 2$ skeletal electrons. This assumes that each vertex atom contributes three internal orbitals to the skeletal bonding so that BH and CH vertices provide two and three skeletal electrons, respectively. Two of the $2n + 2$ skeletal electrons for an *n*-vertex *closo* deltahedron are formally allocated to an *n*-center core bond leaving $2n$ electrons to form *n* surface bonds in a canonical structures of a resonance hybrid.[10]

One limitation in the construction of supraicosahedral deltahedral boranes and carboranes is the reluctance of boron and carbon atoms to occupy the degree 6 vertices necessarily present in supraicosahedral deltahedra not composed of fused smaller deltahedra and thus excluding macropolyhedral boranes.[11] In fact, the 13-vertex dicarbaborane 1,2-μ-$(CH_2)_3$-3-Ph-1,2-$C_2B_{11}H_{10}$ is not a deltahedron since it has one tetragonal face to provide degree 4 vertices for both carbon atoms.[3] The problem with boron, and particularly carbon, at degree 6 vertices can be alleviated by introducing metal vertices isolobal and valence isoelectronic to boron and carbon vertices. Shortly after the original discovery of metallaboranes by Hawthorne and coworkers in the 1960s[12] this approach was used to synthesize the 13-vertex[13] and 14-vertex[14] dicobaltadicarbaboranes $CpCoC_2B_{10}H_{12}$ and $Cp_2Co_2C_2B_{10}H_{12}$, respectively (Cp = η^5-C_5H_5). This approach has recently been used for the synthesis of the 15-vertex deltahedral metallaboranes 1,2-$(CH_2)_3C_2B_{12}H_{12}Ru(\eta^6$-arene)[15] and $Cp^*_2Rh_2B_{13}H_{13}$ (Cp^* = η^5-Me_5C_5).[16] Such supraicosahedral metallaboranes have the metal atoms located at degree 6 vertices.

The tendency of metal atoms to occupy degree 6 vertices provides alternatives to the most spherical *closo* deltahedra for metallaboranes having 9 and 10 vertices with a degree 6 vertex for a metal atom. Such deltahedra can be called *isocloso* deltahedra[17] and are obtained from the corresponding *closo* deltahedra by a diamond-square-diamond process[18] converting two degree 5 vertices into a degree 6 and a degree 4 vertex (Fig. 1). The *n*-vertex *isocloso* metallaborane deltahedra typically have $2n$ skeletal electrons rather than the $2n + 2$ skeletal electrons for the most spherical *closo* deltahedra.[19–21] The 11-vertex most spherical *closo* deltahedron can also function as an *isocloso* deltahedron since it necessarily has a degree 6 vertex for a metal atom.[5] Localized bonding models with three-center bonds in some of the deltahedral faces can account for the $2n$ skeletal electrons in the *n*-vertex *isocloso* deltahedral metallaboranes.[22] Such localized bonding models for *isocloso* metallaboranes with $2n$ skeletal electrons do not have the *n*-center core bond found in related localized bonding models for *closo* borane derivatives. Furthermore, the presence of degree 6 vertices naturally favors bonding topologies with three-center bonds in alternate triangular deltahedral faces surrounding the degree 3 vertex. Thus the three internal orbitals from such degree 6 vertices in the Wade–Mingos

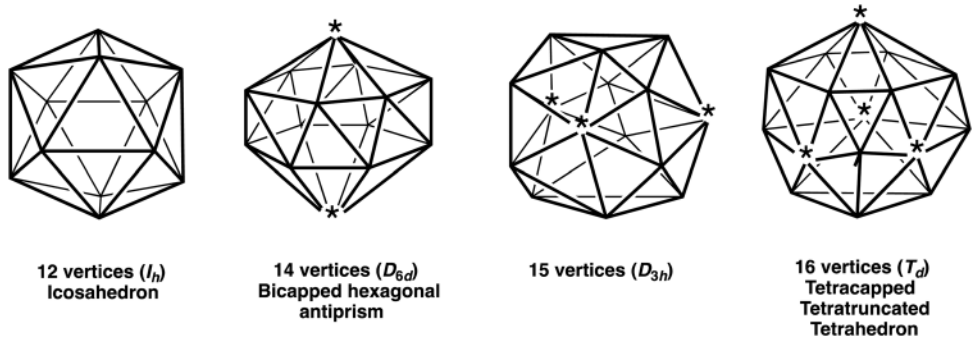

Fig. 2 The four Frank–Kasper deltahedra with the degree 6 vertices starred.

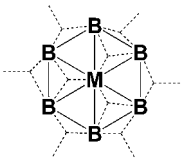

Fig. 3 Interaction of the three internal orbitals (dashed lines) at a degree 6 metal vertex of a metallaborane to form three 3c-2e bonds.

skeletal bonding model[7–9] can naturally form three three-center two-electron bonds (3c-2e) with local three-fold symmetry in the hexagonal pyramidal substructure around such a degree 6 vertex (Fig. 3).

Going beyond the icosahedron to supraicosahedral metallaboranes necessarily increases the number of degree 6 vertices and thus would seem to favor skeletal bonding topology based exclusively on 3c-2e surface bonds without any core bonding. In addition, the larger size of such supraicosahedral deltahedra reduces the orbital overlap provided by the multicenter core bond of the $2n + 2$ skeletal electron bonding model[10] supporting the Wade–Mingos rules[7–9] for the deltahedral *closo* boranes having 12 or fewer vertices. Thus at some point supraicosahedral deltahedra might be expected to become *isocloso* rather than *closo* deltahedra with a preference for $2n$ skeletal electrons rather than $2n + 2$ skeletal electrons for an n-vertex structure. In this connection the experimentally known $Cp^*_2Rh_2B_{13}H_{13}$ having a central 15-vertex Rh_2B_{13} Frank–Kasper deltahedron[16] is a 30 skeletal electron system (= $2n$ for $n = 15$) rather than a 32 skeletal electron system (= $2n + 2$ for $n = 15$) with the metal atoms located at two of the three degree 6 vertices.

This leads to the consideration of structures based on the 16-vertex tetracapped tetratruncated tetrahedron (TTT) which is the largest Frank–Kasper deltahedron (Fig. 2). The three internal orbitals provided by the atoms located at the four tetrahedrally disposed degree 6 vertices of the TTT naturally provide three 3c-2e bonds at each metal vertex leading to a total of 12 3c-2e bonds. The remaining 24 internal orbitals from the 12 degree 5 vertices can then form eight more 3c-2e bonds thereby leading to 3c-2e bonds in a total of 16 of the 28 faces of the TTT.

These considerations suggest that the 16-vertex tetracapped tetratruncated tetrahedron is likely to be an *isocloso* deltahedron with 32 skeletal electrons rather than a *closo* deltahedron with 34 skeletal electrons in a metallaborane structure. This suggestion is reinforced by the observation that 32 is a "magic" number of electrons for a spherical aromatic system since $32 = 2n^2$ for $n = 4$.[23] Thus a spherical TTT metallaborane structure with 32 skeletal electrons is predicted to have a closed shell $1s^2 1p^6 1d^{10} 1f^{14}$ configuration with a large HOMO–LUMO gap. This consideration suggests that group 9 tetrametallaboranes of the type $Cp_4M_4B_{12}H_{12}$ (M = Co, Rh, Ir) with a TTT structure might be a new type of very stable spherical aromatic system.

The only known experimental example of a metallaborane with a 16-vertex tetracapped tetratruncated tetrahedral structure is the recently synthesized[16,24] pentarhodaborane $Cp^*_3Rh_3B_{12}H_{12}Rh(B_4H_9RhCp^*)$ having an external $B_4H_9RhCp^*$ unit functioning as a trihapto ligand rather than a pentahapto Cp* ligand to one

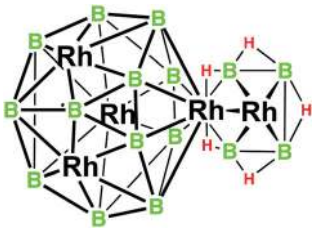

Fig. 4 The experimental $Cp^*_3Rh_3B_{12}H_{12}Rh(B_4H_9RhCp^*)$ structure with the Cp* rings on the rhodium atoms and the terminal hydrogen atoms on the boron atoms omitted for clarity.

of the vertex rhodium atoms in the 16-vertex deltahedron (Fig. 4). The external $B_4H_9RhCp^*$ unit forms an Rh_2B_4 pentagonal pyramid with the rhodium vertex to which it is attached. This species is separated chromatographically in ~15% yield from the mixture obtained by treating $[Cp^*RhCl_2]_2$ with $LiBH_4$·thf in toluene and then heating with BH_3·thf at 105 °C for 5 days.

This interesting, if not seminal, experimental result suggesting a new type of spherical aromatic system has stimulated us to explore the nature of 16-vertex deltahedral tetrametallaborane structures based on the Frank–Kasper tetracapped tetratruncated tetrahedron using modern density functional methods. Our studies include two types of systems:

(1) $Cp_3Rh_3B_{12}H_{12}RhL$ (L = Cp, η^3-allyl, and η^3-B_4H_9RhCp) for comparison with the experimental $Cp^*_3Rh_3B_{12}H_{12}Rh(B_4H_9RhCp^*)$ structure. The η^3-allyl system was chosen as a model because of the trihapto bonding of the $B_4H_9RhCp^*$ ligand in the experimental system.

(2) $[Cp_4M_4B_{12}H_{12}]^z$ (M = Group 8, 9, and 10 metals) in order to establish the preferred structures for various numbers of skeletal electrons.

The tetracapped tetratruncated tetrahedral structure with the four metal atoms at the four degree 6 vertices was chosen as the starting structure. Distortion from the ideal tetrahedral structure was measured by non-equivalent M···M "non-bonding" distances in the macrotetrahedron formed by the four degree 6 metal vertices imbedded in the 16-vertex deltahedron. This latter study not only confirmed the ideal of 32 skeletal electrons for a tetracapped tetratruncated tetrahedral structure but also suggested a new type of 16-vertex polyhedral structure with a central M_4 "macrobutterfly" for the structures with 34 Wadean skeletal electrons (= $2n + 2$ for $n = 16$).

2. Theoretical methods

Geometry optimizations of the 16-vertex tetrametallaboranes started with tetracapped tetratruncated tetrahedral structures having CpM units at each of the four degree 6 vertices and BH groups at the 12 degree 5 vertices. The species investigated included the three rhodium derivatives $Cp_3Rh_3B_{12}H_{12}RhL$ (L = η^5-Cp, η^3-C_3H_5, and η^3-B_4H_9RhCp) related to the experimentally known $Cp^*_3Rh_3B_{12}H_{12}Rh(B_4H_9RhCp^*)$ structure (Table 1). In addition, the transition metal derivatives $[Cp_4M_4B_{12}H_{12}]^z$ (M = Group 8, 9, and 10 metals; $z = -6$ to $+6$) were studied in the Wadean skeletal electron range from 38 in $[Cp_4M_4B_{12}H_{12}]^{2-}$

Table 1 Comparison of tetracapped tetratruncated tetrahedral Rh···Rh distances in the experimental $Cp^*_3Rh_3B_{12}H_{12}Rh(B_4H_9RhCp^*)$ structure with the predicted Rh···Rh distances in model $Cp_3Rh_3B_{12}H_{12}RhL$ (L = η^3-B_4H_9RhCp, Cp, and η^3-C_3H_5) structures

Compound	Local symmetry	Rh···Rh deltahedral distances, Å: $(CpRh)_3$ triangle	Rh···Rh deltahedral distances, Å: From unique Rh
$Cp^*_3Rh_3B_{12}H_{12}Rh(B_4H_9RhCp^*)$ exp.	C_{3v}	3.89, 3.91(2)	3.94(2), 3.96
$Cp_3Rh_3B_{12}H_{12}Rh(B_4H_9RhCp)$ calc.	C_{3v}	3.87, 3.88(2)	3.90, 3.92(2)
$Cp_4Rh_4B_{12}H_{12}$ calc.	T_d	3.88(6)	
$Cp_3Rh_3B_{12}H_{12}Rh(\eta^3\text{-}C_3H_5)$ calc.	C_{3v}	3.88(2), 3.90	3.84, 3.86(2)

(M = Ni, Pd, Pt) to 26 in $[Cp_4M'_4B_{12}H_{12}]^{2+}$ (M′ = Fe, Ru, Os) in order to determine the dependence of the preferred structure on the skeletal electron count. The six non-bonding M···M distances in the optimized structures (Tables 2 and 3) were used as an indication of deviation from the ideal T_d symmetry of the original tetracapped tetratruncated tetrahedron.

Full geometry optimizations were carried out using the B3LYP DFT functional[25–28] coupled with the double zeta 6-31G(d) basis set for all atoms except the second and third row transition metals for which the SDD (Stuttgart Dresden ECP plus DZ) basis set[29] was utilized. The lowest energy structures were then reoptimized at the PBE0/def2-TZVP//SDD level of theory.[30]

All calculations were performed using the Gaussian 09 package[31] with the default settings for the SCF cycles and geometry optimizations. The natures of the stationary points after optimization were checked by calculations of the harmonic vibrational frequencies to insure that genuine minima were obtained. All structures were found to have substantial HOMO–LUMO gaps (see the ESI†).

3. Results and discussion

3.1 $Cp_3Rh_3B_{12}H_{12}RhL$ structures (Table 1 and Fig. 5)

The $Cp_4Rh_4B_{12}H_{12}$ structure has all four rhodium atoms equivalent so the local symmetry of its tetracapped tetratruncated tetrahedron is the full tetrahedral point group (T_d). Minor deviations from ideal T_d symmetry for $Cp_4Rh_4B_{12}H_{12}$ can be related to the mismatch of the five-fold symmetry of the Cp ligand relative to the three-fold local symmetry at the degree 6 rhodium vertices. However, the Rh_4 macrotetrahedron in $Cp_4Rh_4B_{12}H_{12}$ is predicted to have six equivalent 3.88 Å Rh···Rh edges (Table 1).

The $Cp_3Rh_3B_{12}H_{12}RhL$ derivatives in which L ≠ Cp have a unique RhL vertex and three equivalent CpRh vertices so that the local symmetry of the Rh_4B_{12} tetracapped tetratruncated tetrahedron is reduced from T_d to C_{3v} (Fig. 5). As a result the six Rh···Rh distances in these structures are partitioned into two triplets. One triplet consists of the three distances from the unique rhodium atom to the other three rhodium atoms. The other triplet consists of the three edges of the Rh_3 macrotriangle connecting the three equivalent rhodium atoms. Within a given triplet of each type the three distances are found to be equivalent within 0.02 Å. For the $Cp_3Rh_3B_{12}H_{12}Rh(B_4H_9RhCp)$ structure the edges in the macrotriangle Rh···Rh triplet are found to be ∼0.03 Å shorter than the other three Rh···Rh distances from the unique rhodium atom. However, for the $Cp_3Rh_3B_{12}H_{12}Rh(\eta^3\text{-}C_3H_5)$ structure the relative lengths of the two types of Rh···Rh triplets are reversed so that the edges in the macrotriangle Rh···Rh triplet are ∼0.04 Å longer than the three Rh···Rh distances from the unique rhodium atom.

The Rh_2B_4 pentagonal pyramid sharing a rhodium vertex with the central Rh_4B_{12} tetracapped tetratruncated tetrahedron in the $Cp_3Rh_3B_{12}H_{12}Rh(B_4H_9RhCp)$ structures can be dissected

Table 2 The optimized $[Cp_4M_4B_{12}H_{12}]^z$ (M = Pd, Pt, Rh, Ir, Ru, Os; z = −6 to +6) structures. Hydrogen migration is observed in the starred systems

Structure (symmetry)	Metal vertex degrees	M···M distances, Å	M···M distances, Å	Polyhedron M_4 core[a]
		Pd···Pd	Pt···Pt	
$[Cp_4M''_4B_{12}H_{12}]^{2-}$ (C_1)	$4^2 5^2$	3.71, 4.58(2), 4.72(2), 5.59	3.44, 4.59(2), 4.72(2), 5.53	Isolated
$Cp_4M''_4B_{12}H_{12}$ (C_2)	5^4	3.30(2), 3.83(2), 4.75(2)	3.35(2), 3.81(2), 4.76(2)	Trapezoid
$[Cp_4M''_4B_{12}H_{12}]^{2+}$ (C_1)*	$5^2 6^2$	3.88, 3.91, 3.97, 4.01, 4.17, 4.73	3.81, 3.87(2), 3.90, 3.95, 4.82	Butterfly
$[Cp_4M''_4B_{12}H_{12}]^{4+}$ (T_d)	6^4	3.95(6)	3.93(6)	Tetrahed
$[Cp_4M''_4B_{12}H_{12}]^{6+}$ (C_1)*	6^4	4.10, 4.11, 4.12, 4.13, 4.31, 4.36	3.98, 4.00, 4.02, 4.05, 4.19, 4.22	Tetrahed
		Rh···Rh	Ir···Ir	
$[Cp_4M_4B_{12}H_{12}]^{6-}$ (T_d)	6^4	3.81(6)	3.89(6)	Tetrahed
$[Cp_4M_4B_{12}H_{12}]^{4-}$ (T_d)	6^4	3.85(6)	3.89(6)	Tetrahed
$[Cp_4M_4B_{12}H_{12}]^{2-}$ (C_2)	$5^2 6^2$	3.85, 3.86, 3.87, 3.97(2), 4.94	3.86, 3.89(2), 3.94(2), 4.76	Butterfly
$Cp_4M_4B_{12}H_{12}$ (T_d)	6^4	3.88(6)	3.89(6)	Tetrahed
$[Cp_4M_4B_{12}H_{12}]^{2+}$ (C_{3v})*	6^4	3.80, 3.91(3), 3.93(2)	3.78, 3.92(4), 3.93	Tetrahed
$[Cp_4M_4B_{12}H_{12}]^{4+}$ (C_s)	6^4	3.90, 3.93, 3.96, 3.97, 4.01, 4.04	3.83, 3.92, 3.93, 3.96, 4.02, 4.04	Tetrahed
$[Cp_4M_4B_{12}H_{12}]^{6+}$ (C_s)*	6^4	3.95(4), 4.00(2)	3.93(2), 3.96(4)	Tetrahed
		Ru···Ru	Os···Os	
$[Cp_4M'_4B_{12}H_{12}]^{6-}$ (C_{3v})	6^4	3.73(3), 3.91(3)	3.83(3), 3.96(3)	Tetrahed
$[Cp_4M'_4B_{12}H_{12}]^{4-}$ (T_d)	6^4	3.93(6)	3.95(6)	Tetrahed
$[Cp_4M'_4B_{12}H_{12}]^{2-}$ (C_1)	56^3	3.61, 3.79, 3.85, 4.01, 4.04, 5.07	3.64, 3.72, 3.89, 4.02, 4.07, 5.12	Butterfly
$Cp_4M'_4B_{12}H_{12}$ (C_s)	6^4	3.64(2), 3.82(2), 3.93, 3.95	3.77, 3.85(4), 3.98	Tetrahed
$[Cp_4M'_4B_{12}H_{12}]^{2+}$ (C_1)*	6^4	3.48, 3.62, 3.66, 3.82, 3.99, 4.06	3.53, 3.62, 3.68, 3.85, 3.99, 4.09	Tetrahed

[a] Tetrahed = tetracapped tetratruncated tetrahedron; Butterfly = M_4 core with one very long (4.8 to 5.1 Å) M···M distance; Trapezoid = M_4 core with two long ∼4.8 Å distances.

Table 3 The optimized $[Cp_4M_4B_{12}H_{12}]^z$ (M = Ni, Co, Fe; z = −6 to +6) structures. Hydrogen migration is observed in the starred systems

Structure	Symmetry	Skeletal electrons	Metal vertex degrees	Bridging hydrogens	M···M distances, Å	Polyhedron M_4 core[a]
$[Cp_4Ni_4B_{12}H_{12}]^{2-}$	C_2	38	$4^2 5^2$	0	3.60, 4.28(2), 4.46(2), 5.29	Isolated
$Cp_4Ni_4B_{12}H_{12}$	C_2	36	5^4	0	3.34(2), 3.63(2), 4.63(2)	Trapezoid
$[Cp_4Ni_4B_{12}H_{12}]^{2+}$*	C_2	34	$5^2 6^2$	1	3.69, 3.70, 3.76, 3.79, 4.01, 4.38	Tetrahed
$[Cp_4Ni_4B_{12}H_{12}]^{4+}$	C_{3v}	32	6^4	0	3.73(6)	Tetrahed
$[Cp_4Ni_4B_{12}H_{12}]^{6+}$*	C_1	30	6^4	3 C_5H_6 rings	3.83(2), 3.84, 3.88, 3.95, 4.01	Tetrahed
$[Cp_4Co_4B_{12}H_{12}]^{6-}$	D_{2d}	38	6^4	0	3.72(6)	Tetrahed
$[Cp_4Co_4B_{12}H_{12}]^{4-}$	C_2	36	5^4	0	3.72(6)	Tetrahed
$[Cp_4Co_4B_{12}H_{12}]^{2-}$	C_2	34	$5^2 6^2$	0	3.72(3), 3.89(2), 4.86	Butterfly
$Cp_4Co_4B_{12}H_{12}$	D_{2d}	32	6^4	0	3.72(6)	Tetrahed
$[Cp_4Co_4B_{12}H_{12}]^{2+}$*	C_{3v}	30	6^4	1	3.67, 3.69, 3.70, 3.72(3)	Tetrahed
$[Cp_4Co_4B_{12}H_{12}]^{4+}$*	C_1	28	6^4	2	3.59, 3.72, 3.77(2), 3.83, 3.84	Tetrahed
$[Cp_4Co_4B_{12}H_{12}]^{6+}$*	C_3	26	6^4	3 C_5H_6 rings	3.80(3), 3.86(3)	Tetrahed
$[Cp_4Fe_4B_{12}H_{12}]^{6-}$	C_{3v}	34	6^4	0	3.66(3), 3.79(3)	Tetrahed
$[Cp_4Fe_4B_{12}H_{12}]^{4-}$	C_{3v}	32	6^4	0	3.67(3), 3.79(3)	Tetrahed
$[Cp_4Fe_4B_{12}H_{12}]^{2-}$	C_2	30	$5^2 6^2$	0	3.64, 3.69, 3.70, 3.80, 3.87, 4.95	Butterfly
$Cp_4Fe_4B_{12}H_{12}$	D_{2d}	28	6^4	0	3.59, 3.67(4), 3.79	Tetrahed
$[Cp_4Fe_4B_{12}H_{12}]^{2+}$*	C_1	26	6^4	2	3.27, 3.48, 3.58, 3.69, 3.83, 3.89	Tetrahed

[a] Tetrahed = tetracapped tetratruncated tetrahedron; Butterfly = M_4 core with one very long (~5.0 Å) M···M distance; Trapezoid = M_4 core with two long ~4.7 Å "diagonal" distances.

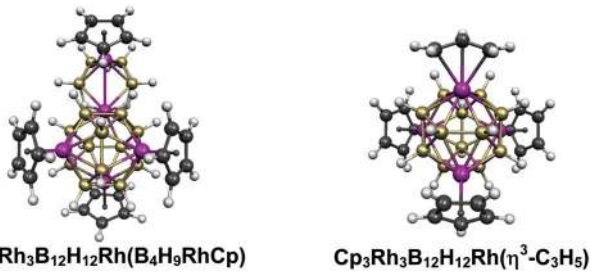

Fig. 5 Comparison of the optimized structures of $Cp_3Rh_3B_{12}H_{12}Rh(B_4H_9RhCp)$ and $Cp_3Rh_3B_{12}H_{12}Rh(\eta^3\text{-}C_3H_5)$ showing the external trihapto ligands on the unique rhodium atom located at the "top" of the central Rh_4B_{12} unit.

into a trihapto η^3-B_4H_9RhCp ligand bonded to the unique rhodium vertex of the large Rh_4B_{12} deltahedron through two boron atoms and one rhodium atom. The calculated Rh–Rh bonding distance of 2.82 Å from the external rhodium atom to the central Rh_4B_{12} deltahedron in the $Cp_3Rh_3B_{12}H_{12}Rh(B_4H_9RhCp)$ structure is close to the corresponding experimental 2.87 Å Rh–Rh distance in $Cp^*_3Rh_3B_{12}H_{12}Rh(B_4H_9RhCp^*)$ determined by X-ray crystallography.

Since the experimental $Cp^*_3Rh_3B_{12}H_{12}Rh(B_4H_9RhCp^*)$ structure has a trihapto η^3-B_4H_9RhCp ligand, we also optimized the simpler $Cp_3Rh_3B_{12}H_{12}Rh(\eta^3\text{-}C_3H_5)$ with a trihapto allyl ligand. The central Rh_4B_{12} deltahedron was found to be very similar to that in the $Cp_4Rh_4B_{12}H_{12}$ structure (Fig. 5). This suggests that a η^3-C_3H_5Rh vertex is a donor of two Wadean skeletal electrons similar to a CpRh vertex. This is reasonable if the rhodium atom in a η^3-C_3H_5Rh vertex has a 16-electron configuration but the rhodium atom in a CpRh vertex unit has an 18-electron configuration. In this connection the rhodium dicarbonyls $CpRh(CO)_2$[32] and $(\eta^3\text{-}C_3H_5)Rh(CO)_2$[33] have similar properties even though the rhodium atom has an 18-electron configuration in the former species but only a 16-electron configuration in the latter species.

3.2 Other transition metal $[Cp_4M_4B_{12}H_{12}]^z$ systems having 26 to 38 skeletal electrons

In an initial attempt to assess the relationship between skeletal electron count and preferred structures for 16-vertex metallaboranes we optimized $[Cp_4M_4B_{12}H_{12}]^z$ of the group 8, 9, and 10 transition metals starting with ideal T_d tetracapped tetratruncated tetrahedral structures with the four CpM units located at the four degree 6 vertices and adjusting the charge (z) to give structures having from 26 to 38 skeletal electrons (Tables 2 and 3). Fig. 6–8 depict the optimized structures of the $[Cp_4M_4B_{12}H_{12}]^z$ derivatives of the second row transition metals palladium, rhodium, and ruthenium, respectively. The corresponding $[Cp_4M_4B_{12}H_{12}]^z$ structures of the first and third row transition metals are similar to those of their second row transition metal congeners and are depicted in the ESI.† The names of the $[Cp_4M_4B_{12}H_{12}]^z$ structures retaining the ideal T_d symmetry of the TTT are indicated in red.

The ideal T_d symmetry of the tetracapped truncated tetrahedron (TTT) with six equivalent macrotetrahedral M···M distances is retained in the 32 skeletal electron structures $Cp_4M_4B_{12}H_{12}$ (M = Co, Rh, Ir), $[Cp_4M'_4B_{12}H_{12}]^{4+}$ (M′ = Ni, Pd, Pt), and $[Cp_4M''_4B_{12}H_{12}]^{4+}$ (M″ = Ru, Os) regardless of the charge. This suggests that 32 skeletal electrons is the "magic number" for stability in a 16-vertex metallaborane based on the most spherical deltahedron. However, 32 (= 2n for n = 16) is the skeletal electron count for an *isocloso* system rather than the skeletal electron count for a *closo* system which would be 34 (= 2n + 2 for n = 16). This can be interpreted as a preference for the *isocloso* skeletal bonding topology with exclusively surface bonding involving canonical structures based on 16 three-center two-electron bonds in selected deltahedron faces.[22] Two features of the TTT would seem to favor *isocloso* bonding topology for this most spherical 16-vertex deltahedron rather than *closo* bonding topology involving canonical structures with a 16-center core bond and 16 two-center two-electron bonds along selected deltahedral edges:[10]

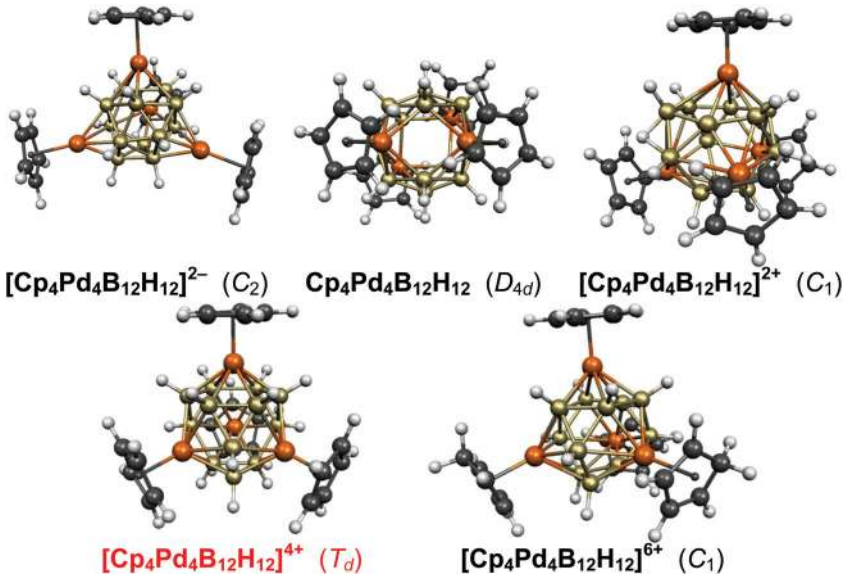

Fig. 6 The lowest energy $[Cp_4Pd_4B_{12}H_{12}]^z$ (z = −2, 0, +2, +4, +6) structures.

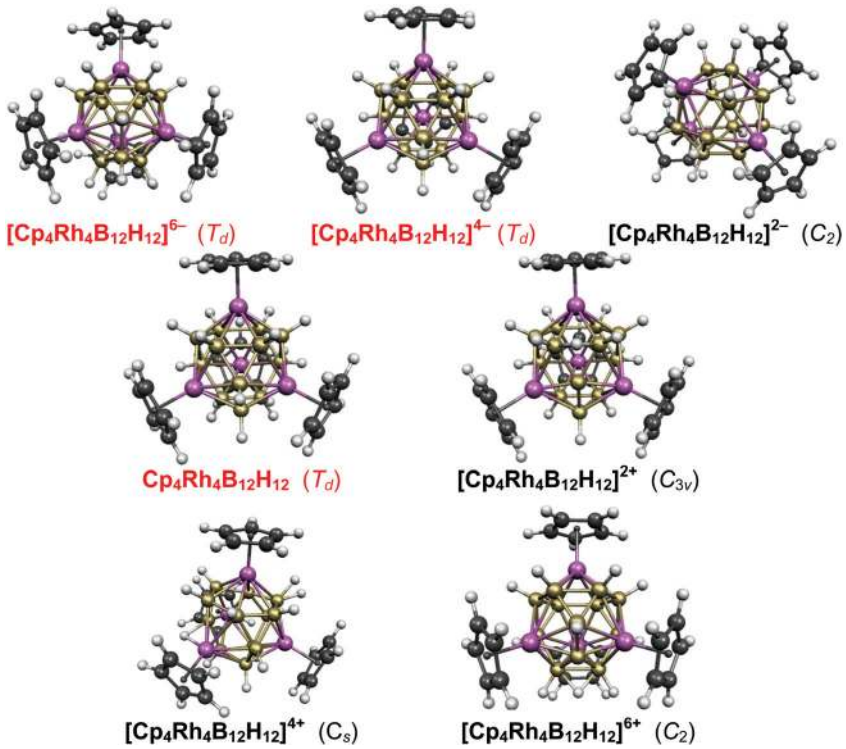

Fig. 7 The lowest energy $[Cp_4Rh_4B_{12}H_{12}]^z$ (z = −6,−4, −2, 0, +2, +4, +6) structures.

(1) The large size of the TTT relative to the regular icosahedron, for example, thereby weakening the unique internal orbital overlap for the multicenter core bond.

(2) The necessary presence of four degree 6 vertices in the TTT favoring orientation of the three internal orbitals from each degree 6 vertex in the centers of alternate faces at the degree 6 vertex (Fig. 3).

Also note that 32 skeletal electrons ($32 = 2n^2$ for $n = 4$) is a magic number for a closed-shell three-dimensional spherical structure[23] in which the 16-orbital 1S + 1P + 1D + 1F manifold is completely filled with electron pairs leading to a closed shell $1S^2 1P^6 1D^{10} 1F^{14}$ configuration.

The one example of a 32 skeletal electron $[Cp_4M_4B_{12}H_{12}]^z$ derivative without a perfect M_4B_{12} TTT of T_d symmetry is the tetrairon tetraanion $[Cp_4Fe_4B_{12}H_{12}]^{4-}$ in which ideal T_d symmetry is distorted to C_{3v} symmetry with three shorter Fe···Fe distances of 3.67 Å and three longer Fe···Fe distances of 3.79 Å.

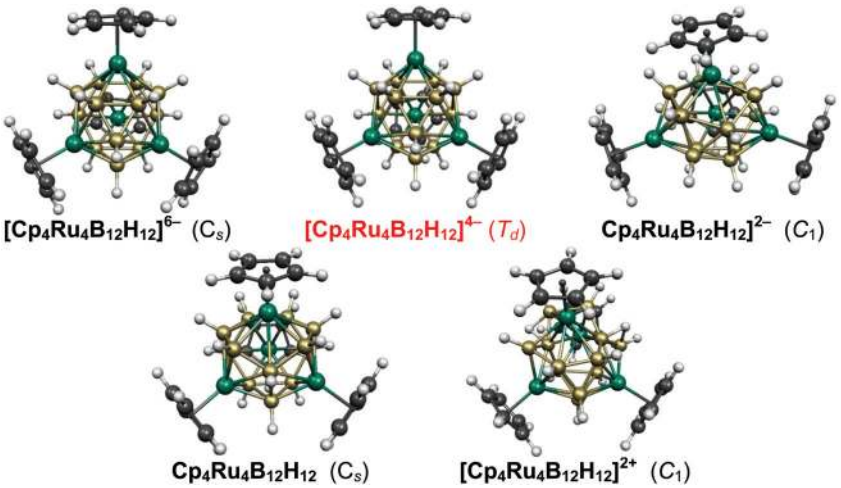

Fig. 8 The lowest energy $[Cp_4Ru_4B_{12}H_{12}]^z$ (z = −6,−4, −2, 0, +2) structures.

The preference of the most spherical 16-vertex TTT for a 32 skeletal electron count for *isocloso* bonding topology rather than a 34 skeletal electron count for *closo* bonding topology is also supported by the preference for a structure very different from the TTT for the 34-skeletal electron systems $[Cp_4M_4B_{12}H_{12}]^{2-}$ (Fig. 7: M = Co, Rh, Ir) and $[Cp_4M''_4B_{12}H_{12}]^{2+}$ (Fig. 6: M″ = Ni, Pd, Pt). Thus attempted optimization of TTT starting structures for these 34-skeletal electron systems leads to considerable distortion. The resulting optimized structures are prolate (elongated) 16-vertex deltahedra with only two of the metal atoms located at degree 6 vertices. The remaining two metal atoms are located at the pair of equivalent degree 5 vertices that are furthest apart leading to a long metal–metal separation of 4.4 to 5.1 Å relating to the prolate nature of this deltahedron. The central M_4 units in these 34 skeletal electron structures can be considered to be distorted macrobutterflies with the long metal–metal separation corresponding to the distance between the butterfly wingtips. In the optimized $[Cp_4M''_4B_{12}H_{12}]^{2+}$ structures (Fig. 6 and 9; M″ = Ni, Pd, Pt). one of the BH hydrogens has migrated to bridge another B–B edge leaving the original boron atom devoid of a terminal hydrogen atom at a relatively flat point on the polyhedral surface. The likewise 34-skeletal electron structures $[Cp_4M'_4B_{12}H_{12}]^{6-}$ (M′ = Ru, Os) retain the TTT topology but with distortion from T_d to C_{3v} (Fig. 8). The six M′···M′ distances of the M'_4 macrotetrahedron are thus partitioned into two groups of three. Thus in $[Cp_4Ru_4B_{12}H_{12}]^{6-}$ three of the Ru···Ru distances are 3.73 Å and the other three Ru···Ru distances are 3.91 Å (Table 2).

Butterfly-type structures are also preferred for the 30-skeletal electron systems $[Cp_4M'_4B_{12}H_{12}]^{2-}$ (M′ = Fe, Ru, Os) with the long wingtip–wingtip distances ranging from 4.95 Å for M′ = Fe to 5.12 Å for M′ = Os (Fig. 8). However, for the likewise 30-skeletal electron systems $[Cp_4M_4B_{12}H_{12}]^{2+}$ (M = Co, Rh, Ir) distorted TTT structures with all M···M distances less than 4.0 Å are found (Fig. 7). In these latter structures one of the B–H hydrogen atoms has migrated to bridge another B–B edge leaving the original boron vertex devoid of a hydrogen atom at a relatively flat point on the polyhedral surface (Fig. 9).

The 30-skeletal electron $[Cp_4M''_4B_{12}H_{12}]^{6+}$ (Fig. 6: M″ = Ni, Pd, Pt) systems exhibit a still different type of structure with hydrogen migrations from three BH vertices to the Cp rings on adjacent metal atoms to give tetrahapto η^4-C_5H_6 cyclopentadiene ligands thereby leaving three bare boron vertices and one unhydrogenated Cp ring. This type of boron-to-Cp hydrogen migration appears to be related to the relatively high +6 charge on the M_4B_{12} cluster since the 26 skeletal electron $[Cp_4M_4B_{12}H_{12}]^{6+}$ (M = Co, Rh, Ir) also exhibit the same pattern of hydrogen migration.

A few 16-vertex tetrametallaboranes with skeletal electron counts other than 32 are found retaining the idealized highly symmetrical T_d TTT structure. Thus the anions $[Cp_4M_4B_{12}H_{12}]^{4-}$ and $[Cp_4M_4B_{12}H_{12}]^{6-}$ (M = Co, Rh, Ir) with 36 and 38 skeletal electrons, respectively, also exhibit the ideal T_d symmetry (Fig. 7)

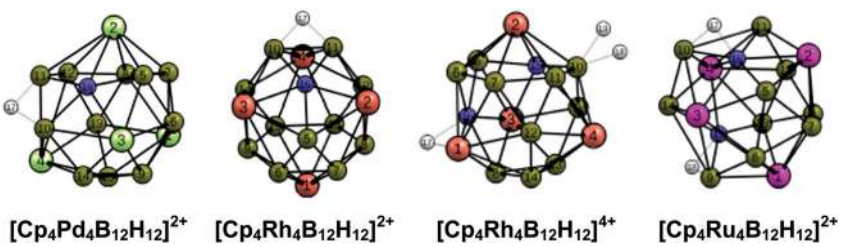

Fig. 9 The M_4B_{12} skeletons of the $[Cp_4M_4B_{12}H_{12}]^z$ structures with bridging hydrogen atoms showing the locations of the bridging hydrogen atoms. Boron atoms providing bridging hydrogen atoms are indicated in blue.

with six equivalent M···M distances from 3.72 Å (M = Co) to 3.89 Å (M = Ir). However, the $Cp_4M''_4B_{12}H_{12}$ (M″ = Ni, Pd, Pt) derivatives, also with 36 skeletal electrons isoelectronic with $[Cp_4M_4B_{12}H_{12}]^{4-}$, are predicted to have a very different type of structure with a central M''_4 macrotrapezoid with two M″···M″ macroedges of length 3.30 Å, two M″···M″ macroedges of 3.83 Å, and two M″···M″ diagonals of length 4.75 Å for M″ = Pd and similar M″···M″ distances for the nickel and platinum derivatives (Fig. 5). The M''_4B_{12} polyhedra in $Cp_4M''_4B_{12}H_{12}$ (M″ = Pd, Pt) are derived from an idealized triple square antiprism of D_{2d} symmetry which is generated by stacking four squares on top of each other with each square staggered at approximately a 45° angle relative to the squares above and below. This polyhedron has a square M''_2B_2 face at each end and 8 triangular faces in each square antiprismatic layer for a total of 24 triangular faces and two square faces. For $Cp_4Ni_4B_{12}H_{12}$ the two equivalent almost square faces with two Ni–B distances of 2.17 Å and two Ni–B distances of 2.21 Å become non-planar rhombi with the two boron atoms bent towards the center and the two nickel atoms bent towards the outside.

The 38-skeletal electron dianions $[Cp_4M''_4B_{12}H_{12}]^{2-}$ (M″ = Ni, Pd, Pt) (Fig. 6) have a very different structure than the regular T_d structure of the isoelectronic hexaanions $[Cp_4M_4B_{12}H_{12}]^{6-}$ (M = Rh, Ir) despite the same number of skeletal electrons. Thus in $[Cp_4M''_4B_{12}H_{12}]^{2-}$ (M″ = Ni, Pd, Pt) the four metal atoms may be regarded as caps on two tetragonal faces and two pentagonal faces of an underlying B_{12} polyhedron and thus have degrees of 4 and 5, respectively. The M″···M″ distances in $[Cp_4M''_4B_{12}H_{12}]^{2-}$ are very long with only one such distance shorter than 4.2 Å.

The highly hypoelectronic 26-skeletal electron dications $[Cp_4M'_4B_{12}H_{12}]^{2+}$ (M′ = Fe, Ru, Os) are the only systems in which the low-energy structures have hydrogen atoms bridging M–B edges rather than B–B edges (Fig. 7 and 9). Each bridge of this type brings two additional electrons from an original external lone pair on the metal atom into the skeletal bonding. Thus with two such hydrogen atoms bridging M–B edges the dications $[Cp_4M'_4B_{12}H_{12}]^{2+}$ (M′ = Fe, Ru, Os) become effectively 30 skeletal electron systems.

4. Conclusion

The experimentally known pentarhodaborane $Cp^*_3Rh_3B_{12}H_{12}Rh(B_4H_9RhCp^*)$ as well as the model compounds $Cp_4Rh_4B_{12}H_{12}$ and $Cp_3Rh_3B_{12}H_{12}Rh(\eta^3\text{-}C_3H_5)$ all have a central Rh_4B_{12} 16-vertex Frank–Kasper deltahedron, namely the tetracapped tetratruncated tetrahedron (TTT). However, the 32 skeletal electron count (= $2n$ for n = 16) rather than a 34 skeletal electron count (= $2n$ + 2 for n = 16) for these systems suggests *isocloso* rather than *closo* skeletal bonding topology. This can be a consequence of the large size of this 16-vertex deltahedron. In addition, the four degree 6 metal vertices favor the three-center two-electron surface *isocloso* bonding topology in selected deltahedral faces rather than the multicenter core bond plus two-center two-electron surface bonding *closo* bonding topology. The 32 skeletal electrons (= $2n^2$ for n = 4) of these systems as well as isoelectronic $[Cp_4M''_4B_{12}H_{12}]^{4+}$ (M″ = Ni, Pd, Pt) and $[Cp_4M'_4B_{12}H_{12}]^{4-}$ (M′ = Fe, Ru, Os) suggest a spherical aromatic system with filled 1S + 1P + 1D + 1F molecular orbitals leading to a $1S^21P^61D^{10}1F^{14}$ configuration.

The preferred structures of the 34 skeletal electron systems $[Cp_4M_4B_{12}H_{12}]^{4-}$ (M = Co, Rh, Ir), $[Cp_4M''_4B_{12}H_{12}]^{2+}$ (M″ = Ni, Pd, Pt) are not the most spherical TTT as expected from their $2n$ + 2 skeletal electron count by blind application of the Wade–Mingos rules. Instead these structures have a central prolate (elongated) polyhedron with two degree 6 and two degree 5 metal vertices with a central M_4 macrobutterfly having one long M···M distance of ~5.0 Å between the wingtips. The preferred structures for the still electron richer 36 skeletal electron systems $Cp_4M''_4B_{12}H_{12}$ (M″ = Pd, Pt) are derived from triple square antiprisms with two open M''_2B_2 square faces. A distorted version of this polyhedron is found in the valence isoelectronic 36 skeletal electron first row transition metal derivatives $Cp_4Ni_4B_{12}H_{12}$ and $[Cp_4Co_4B_{12}H_{12}]^{4-}$. However, this polyhedron is not found in the 36 skeletal electron $[Cp_4M_4B_{12}H_{12}]^{4-}$ (M = Rh, Ir), systems which instead have symmetrical central M_4B_{12} TTTs.

For some 16-vertex $[Cp_4M_4B_{12}H_{12}]^z$ systems deviating from the favored 32 skeletal electron count low-energy structures are found in which hydrogen atoms migrate to bridge B–B edges or bend over to bridge M–B edges. In addition, the hypoelectronic hexacations $[Cp_4M_4B_{12}H_{12}]^{6+}$ (M = Co, Rh, Ir; Ni, Pd, Pt) are found to have low-energy structures in which three of the four Cp rings are hydrogenated to give tetrahapto cyclopentadiene $\eta^4\text{-}C_5H_6$ rings leaving three bare boron vertices at point on the polyhedral surface of relatively low curvature.

Conflicts of interest

The authors declare no competing financial interests.

Acknowledgements

Funding from the Romanian Ministry of Education and Research, Grant PN-III-P4-ID-PCE-2016-0089 is gratefully acknowledged. Computational resources were provided by the high performance computational facility of Babeş-Bolyai University (MADECIP, POSCCE, COD SMIS 48801/1862) co-financed by the European Regional Development Fund.

References

1 *Boron Hydride Chemistry*, ed. E. L. Muetterties, Academic Press, New York, 1975.
2 R. N. Grimes, *Carboranes*, Elsevier, Amsterdam, 2011.
3 A. Burke, D. Ellis, B. T. Giles, B. E. Hodson, S. A. Macgregor, G. M. Rosair and A. J. Welch, Beyond the icosahedron: the first 13-vertex carborane, *Angew. Chem., Int. Ed.*, 2003, **42**, 225–228.

4 L. Dong, H.-S. Chen and Z. Xie, Synthesis, reactivity, and structural characterization of a 14-vertex carborane, *Angew. Chem., Int. Ed.*, 2005, **44**, 2128–2131.
5 R. B. King and A. J. W. Duijvestijn, The topological uniqueness of the deltahedra found in the boranes $B_nH_n^{2-}$ ($6 \leq n \leq 12$), *Inorg. Chim. Acta*, 1990, **178**, 55–57.
6 F. C. Frank and J. S. Kasper, Complex alloy structures regarded as sphere packings. 1. Definitions and basic principles, *Acta Crystallogr.*, 1958, **11**, 184–190.
7 K. Wade, The structural significance of the number of skeletal bonding electron-pairs in carboranes, the higher boranes and borane anions, and various transition-metal carbonyl cluster compounds, *J. Chem. Soc. D*, 1971, 792–793.
8 D. M. P. Mingos, A general theory for cluster and ring compounds of the main group and transition elements, *Nat. Phys. Sci.*, 1972, **236**, 99–102.
9 D. M. P. Mingos, Polyhedral skeletal electron pair approach, *Acc. Chem. Res.*, 1984, **17**, 311–319.
10 R. B. King and D. H. Rouvray, A graph-theoretical interpretation of the bonding topology in polyhedral boranes, carboranes, and metal clusters, *J. Am. Chem. Soc.*, 1977, **99**, 7834–7840.
11 J. D. Kennedy, Macropolyhedral metallaboranes—aspects of preparation, constitution, and structure, *Coord. Chem. Rev.*, 2016, **323**, 71–86.
12 K. P. Callahan and M. F. Hawthorne, Ten years of metallocarboranes, *Adv. Organomet. Chem.*, 1976, **14**, 145–186.
13 D. F. Dustin, G. B. Dunks and M. F. Hawthorne, Novel 13-vertex metallocarborane complexes formed by polyhedral expansion of 1,2-dicarba-closo-dodecaborane(12) ($1,2\text{-}B_{10}C_2H_{12}$), *J. Am. Chem. Soc.*, 1973, **95**, 1109–1115.
14 W. J. Evans and M. F. Hawthorne, Synthesis of fourteen vertex metallocarboranes by polyhedral expansion, *J. Chem. Soc., Chem. Commun.*, 1974, **0**, 38–39.
15 R. D. McIntosh, D. Ellis, G. M. Rosair and A. J. Welch, A 15-Vertex Heteroborane, *Angew. Chem., Int. Ed.*, 2006, **45**, 4313–4316.
16 D. K. Roy, R. Mondal, P. Shakhari, R. S. Anju, K. Geetharam, S. M. Mobin and S. Ghosh, Supraicosahedral polyhedra in metallaboranes: synthesis and structural characterization of 12-, 15-, and 16-vertex rhodaboranes, *Inorg. Chem.*, 2013, **52**, 4705–6712.
17 J. D. Kennedy, Structure and bonding in some recently isolated metallaboranes, *Inorg. Chem.*, 1986, **25**, 111–112.
18 W. N. Lipscomb, Framework rearrangement in boranes and carboranes, *Science*, 1966, **153**, 373–378.
19 J. Bould, J. D. Kennedy and M. Thornton-Pett, Ten-vertex metallaborane chemistry. Aspects of the iridadecaborane closo → isonido → isocloso structural continuum, *J. Chem. Soc., Dalton Trans.*, 1992, 563–576.
20 J. D. Kennedy, in *The Borane-Carborane-Carbocation Continuum*, ed. J. Casanova, Wiley, New York, 1998, ch. 3, pp. 85–116.
21 B. Štibr, J. D. Kennedy, E. Drdáková and M. Thornton-Pett, Nine-vertex polyhedral iridamonocarbaborane chemistry. Products of thermolysis of $[(CO)(PPh_3)_2IrCB_7H_8]$ and emerging alternative cluster-geometry patterns, *J. Chem. Soc., Dalton Trans.*, 1994, 229–236.
22 R. B. King, Topological aspects of the skeletal bonding in 'isocloso' metallaboranes containing ''anomalous'' numbers of skeletal electrons, *Inorg. Chem.*, 1999, **38**, 5151–5153.
23 A. Hirsch, Z. Chen and H. Jiao, Spherical aromaticity in I_h symmetrical fullerenes: the $2(N+1)^2$ rule, *Angew. Chem., Int. Ed.*, 2000, **39**, 3915–3917.
24 D. K. Roy, S. K. Bose, R. S. Anju, B. Mondal, V. Ramkumar and S. Ghosh, Boron beyond the icosahedral barrier: A 16-vertex metallaborane, *Angew. Chem., Int. Ed.*, 2013, **52**, 3222–3226.
25 S. H. Vosko, L. Wilk and M. Nusair, Accurate spin-dependent electron liquid correlation energies for local spin density calculations: a critical analysis, *Can. J. Phys.*, 1980, **58**, 1200–1211.
26 A. D. Becke, Density-functional thermochemistry. III. The role of exact exchange, *J. Chem. Phys.*, 1993, **98**, 5648–5652.
27 P. J. Stephens, F. J. Devlin, C. F. Chabalowski and M. J. Frisch, Ab initio calculation of vibrational absorption and circular dichroism spectra using density functional force fields, *J. Phys. Chem.*, 1994, **98**, 11623–11627.
28 C. Lee, W. Yang and R. G. Parr, Development of the Colle-Salvetti correlation-energy formula into a functional of the electron density, *Phys. Rev. B: Condens. Matter Mater. Phys.*, 1998, **37**, 785–789.
29 C. Adamo and V. Barone, Toward reliable density functional methods without adjustable parameters: the PBE0 model, *J. Chem. Phys.*, 1999, **110**, 6158–6169.
30 D. G. Truhlar and Y. Zhao, The M06 suite of density functionals for main group thermochemistry, thermochemical kinetics, noncovalent interactions, excited states, and transition elements: two new functionals and systematic testing of four M06-class functionals and 12 other functionals, *Theor. Chem. Acc.*, 2008, **120**, 215–241.
31 Gaussian 09 (Revision E.01), Gaussian, Inc., Wallingford, CT, 2009. The complete reference is given in the ESI†.
32 E. O. Fischer and K. Bittler, Cyclopentadienyl-rhodium-dicarbonyl, *Z. Naturforsch.*, 1961, **16b**, 335–336.
33 S. O'Brien, Dicarbonyl-π-allylrhodium, *Chem. Commun.*, 1968, 757–759.

